Responses of hair follicle–associated structures to loss of planar cell polarity signaling

Hao Chang[a,b] and Jeremy Nathans[a,b,c,d,1]

Departments of [a]Molecular Biology and Genetics, [c]Neuroscience, and [d]Ophthalmology and [b]The Howard Hughes Medical Institute, The Johns Hopkins University School of Medicine, Baltimore, MD 21205

Contributed by Jeremy Nathans, January 22, 2013 (sent for review December 27, 2012)

The mammalian hair follicle unit consists of a central follicle and a series of associated structures: sebaceous glands, arrector pili muscles, Merkel cells, and sensory nerve endings. The architecture of this multicellular structure is highly polarized with respect to the body axes. Previous work has implicated Frizzled6 (Fz6)-mediated planar cell polarity (PCP) signaling in the initial specification of hair follicle orientation. Here we investigate the origin of polarity information among structures within the hair follicle unit. Merkel cell clusters appear to have direct access to Fz6-based polarity information, and they lose polarity in the absence of Fz6. By contrast, the other follicle-associated structures likely derive some or all of their polarity cues from hair follicles, and as a result, their orientations closely match that of their associated follicle. These experiments reveal the interplay between global and local sources of polarity information for coordinating the spatial arrangement of diverse multicellular structures. They also highlight the utility of mammalian skin as a system for quantitative analyses of biological polarity.

The structures that decorate the body surface of many animals are generally arranged with precise locations, densities, and orientations. Examples include insect cuticular derivatives such as sensory bristles and vertebrate epidermal derivatives such as hairs, feathers, and scales. In mammals, each hair is synthesized within a follicle, an invagination of surface ectoderm in which stem cells, pigment cells, and epidermal cells are arranged in a highly organized fashion around a central hair shaft (1). In general, follicles are positioned in the dermis at an oblique angle to the skin surface, and, at each location, these angles have a definite orientation relative to the body axes or to local anatomic landmarks. For example, on the dorsal trunk of rodents, hair follicles point from rostral to caudal and on the limbs the follicles point from proximal to distal.

In mammals, an additional level of complexity arises from the arrangement of follicle-associated structures: sebaceous glands, arrector pili muscles (APMs), Merkel cells, and cutaneous sensory nerves (1). Two sebaceous glands emerge from each hair shaft at a point roughly halfway along its length and reside symmetrically on each side of the central shaft (2). One end of an APM fiber attaches to the hair follicle below its sebaceous glands; the other end attaches to the epidermis tens to hundreds of micrometers away. APM contraction pivots the follicle about its point of insertion at the skin surface so that the follicle assumes a more nearly vertical orientation. The Merkel cell complex consists of afferent nerve endings and an associated semicircle of specialized epidermal derivatives that surround the largest follicles [guard or tylotrich hairs (3–5)]. Like primary auditory hair cells, with which they share a number of molecular attributes, Merkel cells appear to act as mechanosensors (6). Hair follicles are in direct contact with a variety of morphologically distinct cutaneous sensory afferents (7, 8). For example, one subtype contacts the follicle with a group of 5–10 extended rods aligned along the follicle axis (lanceolate endings), and a second subtype extends branches that wrap multiple times around the follicle (9). In mice, follicles and follicle-associated structures form on different schedules. Guard hair follicles and semicircular Merkel cell clusters are present by embryonic day (E)16, and follicle-associated lanceolate nerve endings are present by postnatal day (P)0, but sebaceous glands and APMs develop postnatally (2, 10–13).

The orientation of surface structures in insects and mammals is controlled, at least in part, by the tissue polarity or planar cell polarity (PCP) system. First defined in *Drosophila*, PCP signaling is mediated by a core set of approximately six genes that form asymmetric cell surface complexes and convey vectorial information from cell to cell within an epithelium (14). In mice, loss-of-function mutations in *Frizzled* (*Fz*)*6* or *Celsr1*, or the semidominant Loop-tail gain-of-function mutation in *Vangl2*—all homologs of core PCP genes in *Drosophila*—lead to aberrant hair follicle orientations (15–19). In $Fz6^{-/-}$ mice, where this phenomenon has been most extensively studied, follicles on the back initially exhibit orientations that appear approximately random. During the first postnatal week, the follicles reorient within the dermis to generate novel hair patterns, including tufts (cow-licks) and whorls (18, 19). Pattern formation appears to reflect the actions of a developmental program that aligns neighboring follicles, thereby creating a patchwork of small-scale patterns that compete as each pattern enlarges and becomes more organized. This local refinement program, which appears to be independent of PCP signaling, is also active in WT mice, but its effects are not as dramatic as in $Fz6^{-/-}$ mice. In WT mice, follicle orientations in late fetal life are within 10–20° of their mature values, and therefore, their postnatal orientations change relatively little.

In the present study, we take advantage of the 2D structure of the skin and the presence of large numbers of follicles to provide a quantitative analysis of the responses of follicle-associated structures to PCP signaling and to the local refinement process. In particular, we assess in both WT and $Fz6^{-/-}$ backgrounds the relative orientations of follicles and follicle-associated structures, as well as the relationship between the orientations of these structures and the anatomic axes of the mouse to determine whether the orientations of the various follicle-associated

Significance

In mammals, hair follicles reside in the skin together with a set of follicle-associated structures: sebaceous glands, nerve fibers, specialized sensory cells, and muscle fibers. In general, the follicle and its associated structures are precisely oriented with respect to the body axes. The present study shows that, in mice genetically engineered to lack the follicle orienting system, the follicle-associated structures—with the exception of the specialized sensory cells—acquire an orientation that matches that of the follicle. These experiments imply that hair follicles communicate local orienting information to most of their associated structures.

Author contributions: H.C. and J.N. designed research; H.C. performed research; H.C. and J.N. analyzed data; and H.C. and J.N. wrote the paper.

The authors declare no conflict of interest.

[1]To whom correspondence should be addressed. E-mail: jnathans@jhmi.edu.

structures are governed by global polarity cues or by the local polarity of the follicle with which they are associated. These experiments shed light on a fundamental question in developmental biology: how a complex multicellular structure—in this case, the hair follicle unit—coordinates the spatial orientations of its component parts.

Results

Sebaceous Glands. Sebaceous glands can be visualized with lipophilic dyes such as Oil red O. However, in flat mounts of full-thickness skin, this staining can be obscured by dermal fat, which also binds lipophilic dyes. To circumvent this problem, we identified two regions of adult skin—on the dorsal surface of the feet and on the tail—that have minimal fat and are therefore especially suitable for the analysis of sebaceous gland orientation. The dorsal surface of the foot has the further advantage that follicles in this region reproducibly form a single whorl in $Fz6^{-/-}$ mice (15), thus providing a set of follicles that encompass the full range of orientations for quantitative analysis.

Flat-mounted skins from the hind feet of P21 WT and $Fz6^{-/-}$ mice, each carrying a follicle-specific *Keratin (K)17-GFP* transgene (20), were stained with Oil red O and imaged for both GFP and Oil red O (Fig. 1 *A–F*). (Throughout this paper, $Fz6^{+/+}$ and $Fz6^{+/-}$ are interchangeably referred to as WT because both exhibit the WT pattern of follicle orientations.) In these and other experiments described below, P21 was chosen as the optimal age for analysis because this corresponds to the nadir of skin pigmentation during the first telogen cycle (21–23). The highly uniform proximal-to-distal orientation of hair follicles is apparent on the dorsal surface of WT feet (Fig. 1*B*), as is the whorl on the dorsal surface of $Fz6^{-/-}$ feet (Fig. 1*E*). It is also apparent that each follicle is associated with a pair of symmetrically placed sebaceous glands. The orientations within the plane of the skin of 120 follicles and their associated sebaceous glands were determined for WT and $Fz6^{-/-}$ skins (Fig. 1*G*). For both genotypes, the orientation of each pair of sebaceous glands—defined as the line of symmetry between the pair—and the orientation of the associated follicle is highly correlated, with a mean angular difference of $4 \pm 3°$ (mean ± SD) for WT and $6 \pm 5°$ for $Fz6^{-/-}$. This tight spatial coupling presumably reflects the origin of the sebaceous gland as an outgrowth from a follicle-derived progenitor pool and the resulting physical connection of each gland with the follicle from which it originates (2).

In flat mounts of WT tail skin, Oil red O staining reveals a highly ordered arrangement in which triplets of follicles and their paired sebaceous glands are associated with an oval-shaped zone of melanin pigmentation (Fig. 2 *A* and *C*). These clusters are arranged in lateral rows, with neighboring rows exhibiting an offset in phase of 180°, i.e., hexagonal packing. In $Fz6^{-/-}$ tail skin, this arrangement is disorganized in several ways: the number of follicles per cluster varies, adjacent clusters frequently exhibit partial or complete fusion, the zones of pigmentation lack a fixed relationship to the position of nearby follicles, and the lateral alignment of follicle clusters is degraded (Fig. 2 *B* and *D*). In contrast to the situation on the foot, the position and symmetry of sebaceous glands are affected in $Fz6^{-/-}$ tail skin, with some

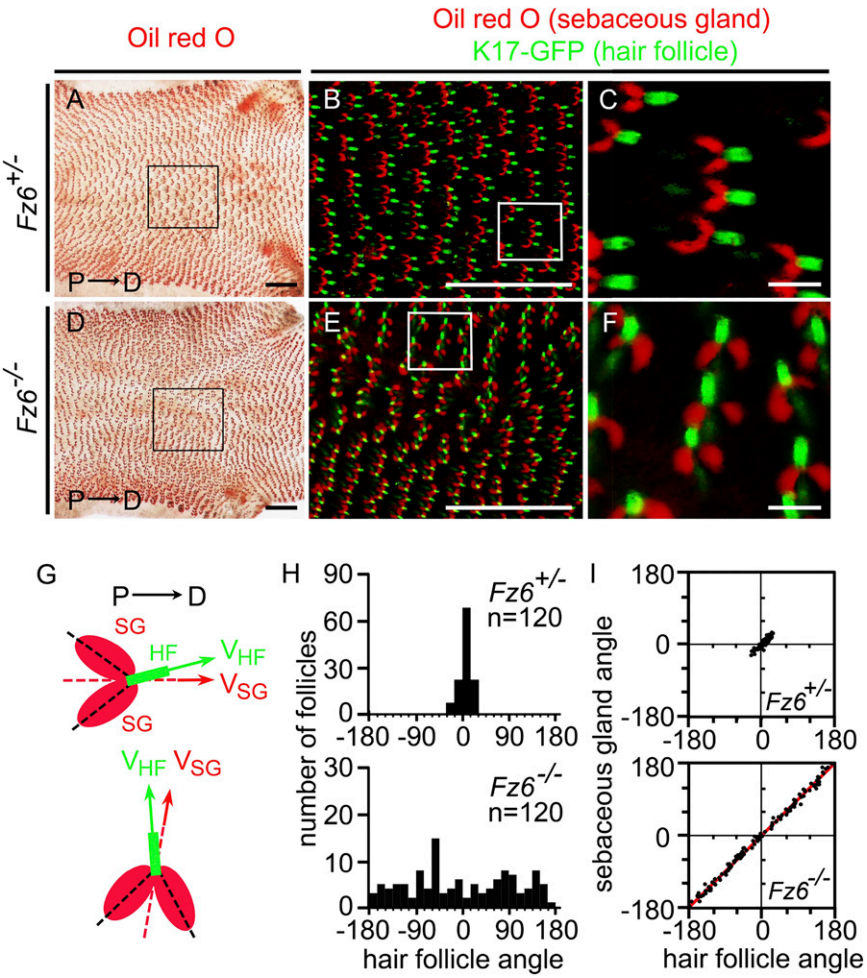

Fig. 1. Orientation of hair follicles and sebaceous glands on the hind paws of P21 $Fz6^{+/-}$ and $Fz6^{-/-}$ mice. (*A–F*) Sebaceous glands were visualized in flat mount Oil red O–stained skin using transmitted light (*A* and *D*) and pseudocolored to red (*B, C, E,* and *F*). Hair follicles were visualized by the fluorescence of *K17-GFP* (green). In the fluorescent images, the confocal Z-stack encompasses only the outer (i.e., most superficial) half of each follicle. A 2.1 × 1.7-mm region centered over the hair whorl in $Fz6^{-/-}$ mice is boxed in *D* and enlarged in *E*; the corresponding region in the $Fz6^{+/-}$ control is boxed in *A* and enlarged in *B*. These regions from six $Fz6^{+/-}$ hind paws and six $Fz6^{-/-}$ hind paws were scored for the orientations of sebaceous glands and hair follicles as shown in *G* and *H*. Boxed regions in *B* and *E* are enlarged in *C* and *F*, respectively. Proximal is to the left and distal is to the right. (*G*) Diagram showing the measurement of sebaceous gland and hair follicle angles relative to the proximal-distal axis. Green, hair follicle (HF); red, sebaceous gland (SG); V_{HF}, hair follicle vector; V_{SG}, sebaceous gland vector. (*H*) Histograms showing that $Fz6^{+/-}$ control hair follicles have orientations with a maximum range from −30° to 30°, and $Fz6^{-/-}$ hair follicles near the whorl center span the full range of orientations. (*I*) Scatter plots showing the relationship between the orientations of hair follicle and their associated sebaceous glands angles. An angle of 0° corresponds to the proximal-to-distal direction. Red line, Deming regression line. (Scale bars, 1 mm in *A, B, D,* and *E*; 100 μm in *C* and *F*.)

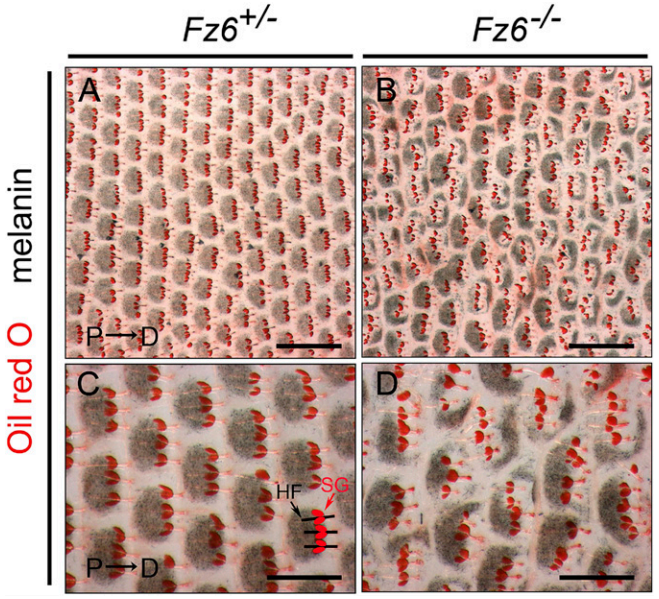

Fig. 2. Organization of follicles, sebaceous glands, and skin pigmentation on the tail. (*A–D*) Oil red O staining of flat mounted P21 tail skin from WT (*A* and *C*) and *Fz6*$^{-/-}$ (*B* and *D*) mice. Proximal is to the left and distal is to the right. One cluster of three follicles, each with its lateral pair of sebaceous glands, is shown schematically in *C*. Disorganization of these clusters, with asymmetries in the paired sebaceous glands and aberrant numbers and locations of follicles, is evident throughout *B* and *D*. HF, hair follicle; SG, sebaceous gland. (Scale bars, 1 mm in *A* and *B*; 500 μm in *C* and *D*.)

follicles exhibiting sebaceous glands of different size or, in some cases, only a single sebaceous gland. These data indicate that PCP signaling is required—either directly or indirectly—for multiple aspects of the nearly crystalline arrangement of epidermal structures in the tail skin.

APMs. An initial survey of different skin regions showed that follicles on the foot lack APMs, whereas each follicle on the back is associated with an APM. For quantitative analyses, APMs were visualized in flat-mount P21 back skin by immunostaining for anti-smooth muscle actin (SMA), hair follicles were visualized with anti-GFP antibodies (the mice carry the *K17-GFP* transgene), and the skin was clarified after immunostaining with 2:1 benzyl benzoate:benzyl alcohol (BBBA). The resulting Z-series confocal images reveal the full trajectories of hair follicles and their associated APMs (Fig. 3). To increase the frequency of encountering follicles with aberrant orientations on the backs of adult *Fz6*$^{-/-}$ mice, we incorporated a recessive modifier allele, referred to as the *ridge* allele, that we recently discovered serendipitously and that produces whorls and ridges at nearly 100% efficiency when combined with homozygous loss of *Fz6*. By contrast, *Fz6*$^{-/-}$ mice maintained on a mixed C57BL/6 × 129 background, which are not homozygous for the *ridge* allele, exhibit multiple back whorls and ridges only during the first 2 postnatal wk. In most of these mice, the follicles progressively reorient to become nearly parallel to the anterior-posterior (A-P) axis by P21. At present, the molecular identity of the *ridge* modifier is unknown.

In WT back skin at P21, follicles are aligned with the A-P axis, and follicle and APM orientations are highly correlated, with a mean angular difference of only 10 ± 9° (mean ± SD; Fig. 3 *A–E*). To assess the full range of possible APM and follicle orientations, we analyzed three regions of P21 *Fz6*$^{-/-}$*;ridge/ridge* back skin with very different follicle orientations. One territory, labeled A to P in Fig. 3 *F–J*, is populated by follicles oriented from anterior to posterior. Although the follicle orientations at this time point closely resemble those of the WT sample, the *Fz6*$^{-/-}$*;ridge/ridge* follicles have arrived at these orientations by a more circuitous route because their orientations were highly variable 3 wk earlier (18, 19). As seen in Fig. 3 *F–J*, the APMs and follicles in this zone are relatively well aligned, with a mean angular difference of 13 ± 12°, only slightly larger than the WT control. A second territory, labeled P to A in Fig. 3 *K–O*, is populated by follicles that are oriented from posterior to anterior, i.e., they are reversed 180° to the WT orientation. By visual inspection, some of the associated APMs appear less well aligned compared with WT APMs, with some individual muscle fibers showing a pronounced bend. For this cohort, the mean angular difference between follicles and APMs is 13 ± 13°.

A third territory, encompassing the center of a whorl, exhibits a number of distinctive features (Fig. 3 *P–T*). As described by Wang et al. (19) and seen in Fig. 3*Q* (arrowheads), follicles close to the center of a whorl are often bent, suggesting that in this region the local alignment mechanism drives a more extensive reorientation. Some APMs close to the center of the whorl are also bent, suggesting that they are undergoing a parallel process of reorientation. In this territory, the mean angular difference between follicles and APMs (46 ± 35°) is substantially higher than in the WT control. Visual inspection of the vector schematic (Fig. 3*S*) and scatter plot (Fig. 3*T*) show that there is also a systematic deviation of APM angles toward the A-P axis. By contrast, follicle angles evenly populate the full 360°, as expected for the constituents of a circularly symmetric whorl. As a result, the best-fitting line for the APM vs. follicle angle scatter plot has a slope of 29° from the horizontal [red line in Fig. 3*T*; calculated from the Deming regression line (24)].

We can attempt an interpretation of these data by considering the spatial relationship between the points of APM attachment on the follicle and at the epidermis, as well as the relationship between follicle orientation and APM orientation during the period of follicle rotation. As discussed more fully below, APM development begins at ∼P1 and is complete by ∼P5 (13), a time window that largely overlaps the period of follicle rotation in *Fz6*$^{-/-}$ skin. Five possible models encapsulating these relationships are shown in Fig. 3*U*. In WT back skin, the site of APM attachment at the epidermis is located almost directly posterior to the epidermal insertion point of its associated follicle (Fig. 3 *A–E*). The regular arrangement of follicle insertion points at all stages of development suggests that these points are fixed (19). If, in *Fz6*$^{-/-}$ skin, the sites of APM attachment at the epidermis were fixed at the same locations as in WT skin, then the APMs would track the reorienting follicles as diagrammed in model A of Fig. 3*U*. The data appear to rule out this model because it predicts that follicles with fully reversed orientations would be attached to APMs that are substantially shortened, whereas the data show that APM lengths are unaffected when follicle orientations are reversed (cf. Fig. 3 *F–I* and *K–N*). Model B in Fig. 3*U*, which posits a lock-step relationship between follicle orientation and APM insertion point, and model E, which shows the APM developing after all follicle movements have ceased, also appear to be incompatible with the data, as these models fail to account for the discrepancy between follicle and APM orientations near the center of a whorl (Fig. 3 *P–T*).

Instead, the data point to models in which the site of APM attachment at the epidermis is mobile and/or is determined relatively late in follicle development, as seen in models C and D in Fig. 3*U*. These models are consistent with the wide range of APM orientations and with the residual discrepancy between APM and follicle orientations seen in territories, such as the center of a whorl, where follicles likely undergo the greatest reorientation. The discrepancy between APM and follicle orientations at the center of a whorl, quantified by the shallow slope

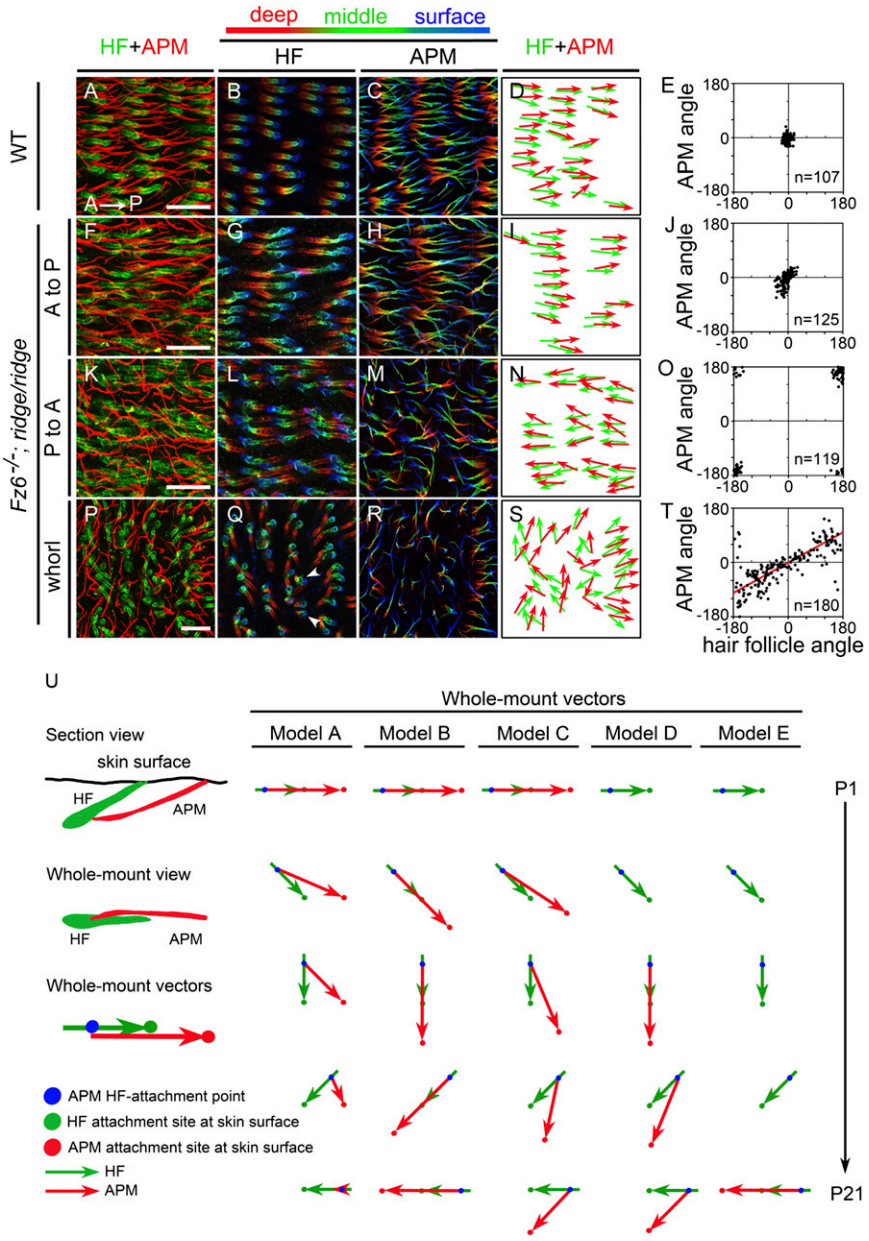

Fig. 3. APM orientations on the back skin of P21 WT and *Fz6*$^{-/-}$*;ridge/ridge* mice. (*A–T*) Follicles and APMs are visualized by flat mount immunostaining for GFP (Alexa Fluor 647, pseudocolored green) and smooth muscle actin (SMA; Alexa Fluor 594, red), respectively. All mice used in this experiment carry a *K17-GFP* transgene. Follicles and APMs are shown in Z-stacked confocal images from WT skin (*A*) and from different regions within a whorl in *Fz6*$^{-/-}$*; ridge/ridge* skin (*F, K*, and *P*). Anterior is to the left and posterior is to the right. P to A (posterior to anterior) and A to P (anterior to posterior) refer to the global orientations of follicles in the regions shown. For each Z-stacked image, follicles (*B, G, L*, and *Q*) and APMs (*C, H, M*, and R) are also shown separately, with deep, middle, and surface layers pseudocolored red, green, and blue, respectively, to more clearly visualize the trajectories of individual fibers. Vector maps (*D, I, N*, and *S*) from these images show the orientations of paired hair follicles (green) and APMs (red). Scatter plots (*E, J, O*, and *T*) show the relationship between the orientations of hair follicles and their associated APMs for skin territories in and near the images shown to the left. In this and all following figures, an angle of 0° corresponds to the anterior-to-posterior direction. (Scale bar, 200 μm.) (*T*) Red line, Deming regression line. (*U*) Models of follicle (green) and APM (red) reorientation on the back skin, shown as a time series from P1 (top) to P21 (bottom) for a follicle that reorients 180°. The models differ with respect to the location, mobility, and time course of development of the APM attachment site (APMAS) at the epithelial surface. Model A: the APMAS is immobile and is located posterior to the site of follicle emergence at the skin surface. Model B: the APMAS rotates so that it always lies along the follicle axis and at the same distance from the follicle. Model C: as in model B, but APMAS rotation lags behind follicle rotation. Model D: the start of APMAS development is delayed relative to the onset of follicle rotation and the APMAS is fixed at a position that is defined by the follicle axis at an intermediate time point in development. Model E: the choice of APMAS occurs after follicle rotation has ceased and the APMAS lies along the follicle axis.

of the scatter plot in Fig. 3*T*, is consistent with the idea that APM movement responds to and lags behind follicle reorientation.

Merkel Cells. As noted in the Introduction, a semicircle of specialized epithelial derivatives (Merkel cells) surrounds the base of each guard hair follicle (Fig. 4*A*). Merkel cells can be labeled either by immunostaining for cytokeratin-8 (CK8) or by in vivo uptake of bulky cationic dyes, such as AM1-43 and AM4-65, that permeate large nonselective cation channels (25) (Fig. 4 B–B″). In comparing WT and *Fz6*$^{-/-}$ back skin at P1 and P14, the Merkel cell distribution exhibits a striking difference: instead of the semicircle of Merkel cells seen in WT skin, Merkel cells in *Fz6*$^{-/-}$ skin are arranged in a circle (Fig. 4 *C–H*).

We quantified this phenotype using three measurements on 60 WT and 60 *Fz6*$^{-/-}$ Merkel cell clusters at P1. First, we measured the angle, centered on the follicle, of the largest inter-Merkel cell gap within each cluster (Fig. 4 *I* and *J*, *Left*); second, we counted the number of Merkel cells in the anterior and posterior halves of the cluster, as determined by bisecting the image with a line centered on the follicle and oriented perpendicular to the A-P axis (Fig. 4 *I* and *J*, *Center*); and third, we counted the number of Merkel cells in the proximal and distal territories of the cluster, with these territories determined by bisecting the image with a line centered on the follicle and oriented perpendicular to the follicle axis (Fig. 4 *I* and *J*, *Right*). The first method assesses the completeness of the circle of Merkel cells irrespective of the orientation of the Merkel cluster or its follicle. The second and third methods assess the extent to which asymmetry in the Merkel cell distribution conforms to the A-P axis or to follicle orientation, respectively. All three methods show highly significant differences between WT and *Fz6*$^{-/-}$ Merkel cell arrangements, with no evidence for spatial asymmetry in the Merkel cell clusters of *Fz6*$^{-/-}$ mice. Importantly, these data show that, in the absence of *Fz6*, the asymmetry of the Merkel cell cluster is absent at P1, shortly after Merkel cells have clustered around the central follicle (see below). If, as suggested by Nurse and Diamond (3), the semicircular arrangement of Merkel cells is important for

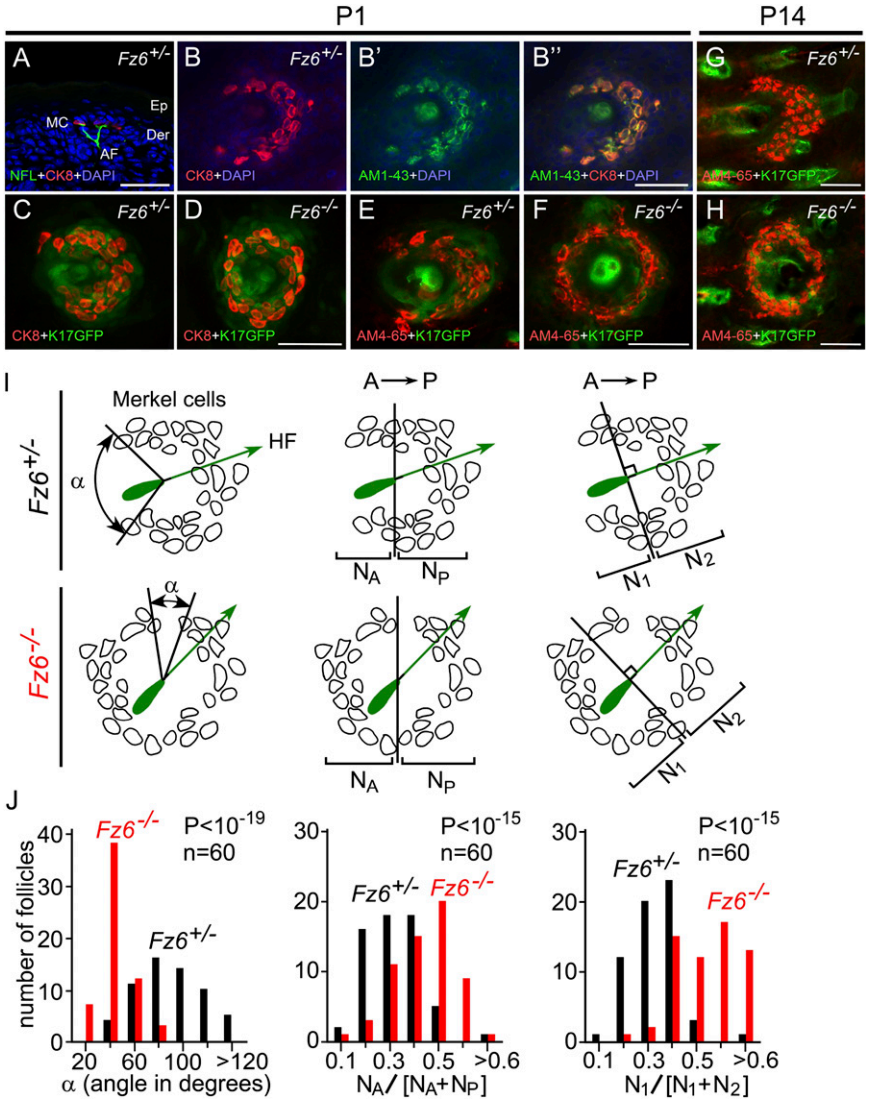

Fig. 4. Morphology of Merkel cell clusters in P1 and P14 WT and $Fz6^{-/-}$ mice. (*A*) Merkel cells and afferent sensory fibers in a vertical section of P1 $Fz6^{+/-}$ skin visualized with cytokeratin 8 (CK8), anti-neurofilament immunostaining, and DAPI staining. AF, afferent fiber; Der, dermis; Ep, epidermis; MC, Merkel cell. (*B*) Flat mount skin after systemic AM1-43 dye exposure shows labeling of Merkel cells by both CK8 immunostaining and AM1-43. (*C–F*) Merkel cells in $Fz6^{+/-}$ flat mount skin form a semicircular cluster around the guard follicle, with an opening to the anterior (*C* and *E*), whereas Merkel cells in $Fz6^{-/-}$ skin form a closed circular cluster around the guard follicle (*D* and *F*). (*G* and *H*) Arrangement of $Fz6^{+/-}$ and $Fz6^{-/-}$ Merkel cell at P14, visualized with AM4-65 in flat mount skin. In *B–H*, anterior is to the left and posterior is to the right. (Scale bar, 50 μm.) (*I*) Diagrams showing the measurement of the open angles of Merkel cell clusters and the distributions of Merkel cells around guard follicles in flat mount skin at P1. (*Left*) For each Merkel cell cluster, the opening angle is measured by connecting the two most distantly separated Merkel cells to the center of the hair shaft within the same Z-plane. (*Center*) Number of Merkel cells anterior (N_A) or posterior (N_P) to a line bisecting the follicle at right angles to the A-P axis. (*Right*) Number of Merkel cells proximal (N_1) or distal (N_2) to a line bisecting the follicle at right angles to the axis of the follicle. (*J*) Bar graphs showing the orientations of Merkel cell clusters and the distribution of Merkel cells within each cluster as diagrammed in *I*. In $Fz6^{-/-}$ mice, Merkel cell clusters have a smaller open angle and Merkel cells are more symmetrically arranged with respect to both the body axis and their associated follicle axis compared with $Fz6^{+/-}$ controls.

sensing directional stimuli, then the circularly symmetric arrangement in $Fz6^{-/-}$ skin would likely impair this function.

Follicle-Associated Nerve Endings. Any assessment of the geometry of hair follicle innervation faces the challenge that each follicle is innervated by multiple cutaneous sensory afferents, thus precluding the use of neurofilament immunostaining or other non-selective methods for visualizing the structure of individual afferents (11). Recently, Badea et al. (26) described a genetically directed approach for sparse histochemical labeling of individual cutaneous afferents using tamoxifen-controlled neuron-specific Cre recombination to activate the expression of a membrane-anchored alkaline phosphatase (AP) reporter. This system combines an *IRES-CreER* knock-in at the *Neurofilament Light Chain* gene [*NFL-CreER* (27)] and Cre-controlled transcription of an *AP* knock-in at the *Brn3a* gene, which is widely expressed in dorsal root ganglion (DRG) neurons. In the present experiments, Cre-mediated recombination was transiently activated by maternal injection of tamoxifen at day 14 of gestation. We used this bipartite genetic system in both a conventional $Fz6^{-/-}$ background and a $Fz6^{-/-}$;*ridge*/*ridge* background and focused on a relatively common class of sensory afferents with C-shaped endings that contact hair follicle shafts. These arbors are heterogeneous in size, and the C-shaped endings are decorated with longitudinal lanceolate specializations and are distinct from the endings that contact Merkel cell clusters.

P2 back skins from $Fz6^{+/-}$;$Brn3a^{CKOAP/+}$;*NFLCreER* and $Fz6^{-/-}$;$Brn3a^{CKOAP/+}$;*NFLCreER* littermates that were stained histochemically for AP show similar abundances, sizes, and branching patterns of sensory arbors. At this age, hair follicles in $Fz6^{-/-}$ skin exhibit a variety of orientations, whereas follicles in WT skin are highly organized in an anterior-to-posterior direction. In WT skin the C-shaped sensory endings face anteriorly, whereas in $Fz6^{-/-}$ skin the C-shaped sensory endings exhibit a variety of orientations (Fig. 5 *A* and *B*).

Additionally, in $Fz6^{-/-}$ skin, ∼30% of the follicle-associated nerve endings fully encircle the follicle (O-shaped endings), a morphology that is only rarely observed in the WT (Fig. 5*C*). The C- and O-shaped endings are found on different branches of the same sensory arbor, suggesting that they represent alternate forms of the same type of sensory structure. Both types are located close to the skin surface with the endings largely confined to a plane perpendicular to the follicle axis. The opening of the C-shape faces the bulb of the follicle. The presence of O-shaped endings in $Fz6^{-/-}$ skin implies that sensory nerve endings, like Merkel cell clusters, use PCP information, either directly or indirectly, to develop an asymmetric structure.

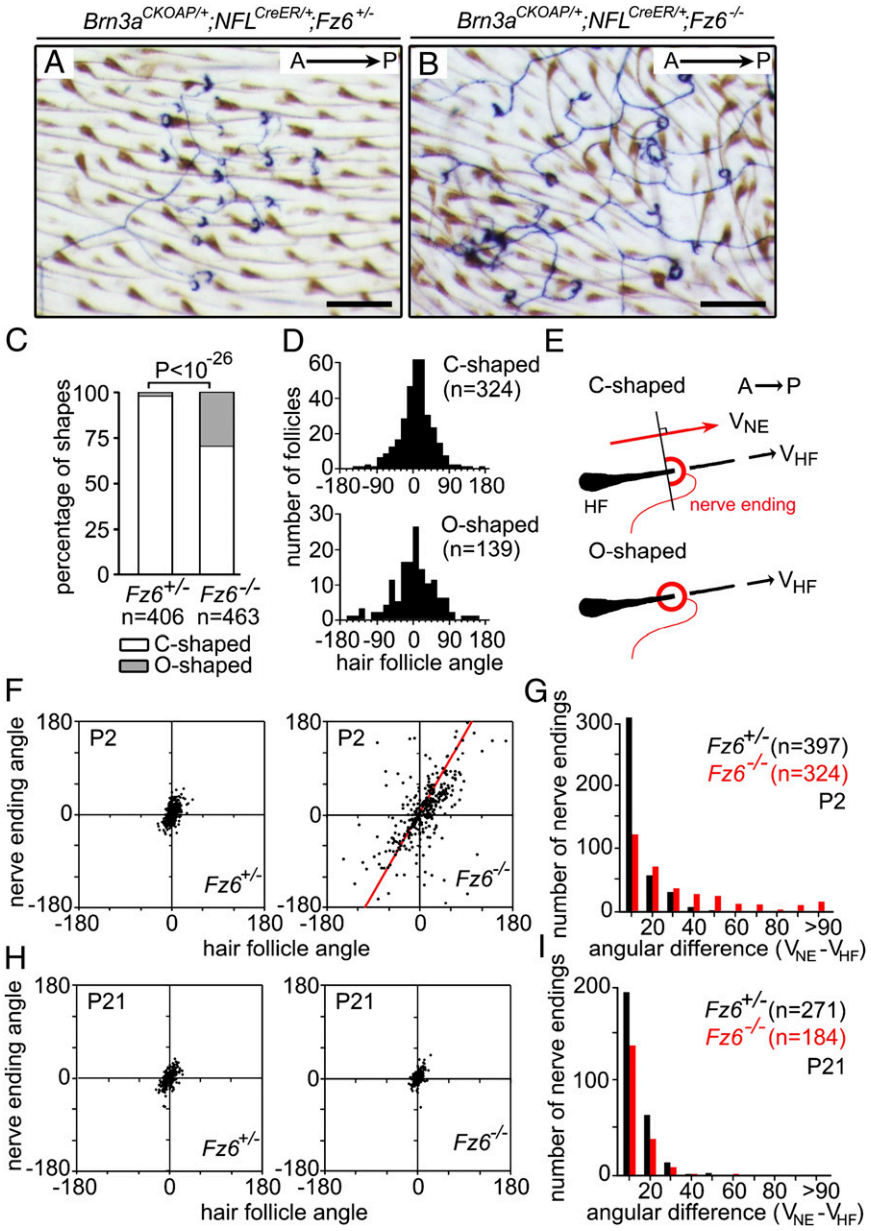

Fig. 5. Morphologies and orientations of C-shaped sensory nerve endings on back skins of WT and *Fz6*$^{-/-}$ mice. (*A* and *B*) Individual sensory arbors with hair follicle–associated endings were visualized in flat mount skin at P2 by AP staining after sparse Cre-mediated recombination in *Brn3a*$^{CKOAP/+}$;*NFL-CreER*;*Fz6*$^{+/-}$ and *Brn3a*$^{CKOAP/+}$;*NFL-CreER*;*Fz6*$^{-/-}$ littermates. In addition to C-shaped endings, many O-shaped endings are found in *Fz6*$^{-/-}$ skin. The high density of innervated follicles indicates that many, and perhaps all, are of the zigzag and/or awl/auchenne types. (Scale bar, 200 μm.) (*C*) Bar graph quantifying the relative number of C- and O-shaped endings in the skins of *Fz6*$^{+/-}$ and *Fz6*$^{-/-}$ mice at P2. (*D*) Histograms showing the orientations of hair follicles that are associated with the C- and O-shaped endings in *Fz6*$^{-/-}$ mice at P2. The A-P axis has an angle of 0°. (*E*) Diagram illustrating the assignment of follicle and C-shaped ending orientations in flat mount skin. V_{NE}, C-shaped nerve ending vector; V_{HF}, hair follicle vector. (*F*) Scatter plot showing the relationship between the orientations of hair follicles and their associated C-shaped nerve endings at P2. Red line, Deming regression line. (*G*) Histogram showing the differences between the orientations of hair follicles and their associated C-shaped nerve endings in WT (black) and *Fz6*$^{-/-}$ (red) mice at P2. (*H*) As in *F*, except at P21. (*I*) As in *G*, except at P21.

In *Fz6*$^{-/-}$ skin, the angular distributions of follicles associated with C- or O-shaped endings were indistinguishable and appeared, in both cases, to constitute a representative sampling of the follicle population (Fig. 5 *D* and *E*). Quantification of the orientations of >300 pairs of follicles/C-shaped endings per genotype showed a tight correlation in WT skin (mean angular difference of 10 ± 8°) and a weaker correlation in *Fz6*$^{-/-}$ skin (mean angular difference of 28 ± 33°) with approximately one-quarter of the *Fz6*$^{-/-}$ pairs exhibiting angular differences of >45° (Fig. 5 *D*, *F*, and *G*).

As noted above in the description of APM orientations, in the absence of the *ridge* allele, most of the follicles on the backs of *Fz6*$^{-/-}$ mice reorient to a nearly parallel configuration by P21. During this postnatal period of follicle reorientation, we observed that C-shaped endings also reorient so that by P21 they have attained the same pairwise concordance with their associated follicles as the P21 WT control, with mean angular differences of 8 ± 7° for both distributions (Fig. 5 *H* and *I*). Interestingly, in *Fz6*$^{-/-}$ mice, during the first 3 wk of postnatal life, there is either a selective removal of O-shaped endings or a conversion of O-shaped to C-shaped endings. Specifically, in the *Fz6*$^{-/-}$ sample at P2, 30% (139/463) of sensory endings were O-shaped, whereas at P21, 1% (2/186) were O-shaped. In the control *Fz6*$^{+/-}$ sample at P2, 2% (9/406) of sensory endings were O-shaped, and at P21, 1% (3/274) were O-shaped. A conversion from an O-shaped to C-shaped ending might represent a maturation process that is coupled to the maturation of follicle orientation.

A more dramatic test of the reorienting capability of C-shaped follicles is afforded by studying *Fz6*$^{-/-}$;*ridge*/*ridge* mice, because at P21 they exhibit large numbers of follicles covering the full range of orientations. Fig. 6*I* shows, in schematic form, the pattern of follicle orientations in the head and back skin of a typical *Brn3a*$^{CKOAP/+}$;*NFLCreER*;*Fz6*$^{-/-}$;*ridge*/*ridge* mouse at P21, and Fig. 6 *A*–*H* shows representative sensory arbors with C-shaped endings from the four territories demarcated by black squares in Fig. 6*I*. The four territories contain follicles with orientations that represent, to first approximation, the four cardinal directions within the plane, and in each case the C-shaped

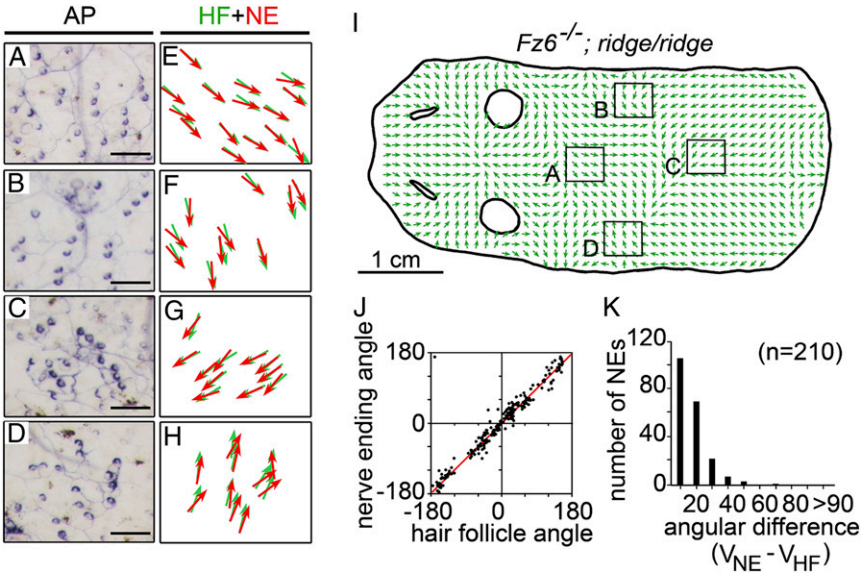

Fig. 6. Orientations of C-shaped sensory nerve endings on back skins of P21 *Fz6*$^{-/-}$;*ridge/ridge* mice. (*A–H*) Examples of individual sensory arbors on the back visualized in flat mount skin by AP staining after sparse Cre-mediated recombination in *Fz6*$^{-/-}$;*ridge/ridge*;*Brn3a*$^{CKOAP/+}$;*NFLCreER* mice. HF, hair follicle; NE, nerve ending. In each case, the orientations of C-shaped endings and follicles are closely matched. (*I*) Diagram of hair follicle orientations on P21 *Fz6*$^{-/-}$;*ridge/ridge*;*Brn3a*$^{CKOAP/+}$;*NFLCreER* back skin showing the locations of the sensory arbors in *A–D*. (*J*) Scatter plot showing the relationship between the orientations of hair follicles and their associated C-shaped nerve endings at P21. Red line, Deming regression line. (*K*) Histogram showing the differences between the orientations of hair follicles and their associated C-shaped nerve endings at P21.

endings have reoriented to almost perfectly match the orientations of their associated follicles (Fig. 6 *E–H*). A compilation of orientations for 210 follicle/C-shaped ending pairs further confirms this observation, with mean angular differences of 12 ± 10° (Fig. 6 *J* and *K*). Taken together, these data imply both a close anatomic coupling between follicles and C-shaped endings and substantial postnatal plasticity that promotes their coordinated reorientation.

Developmental Time Course and Patterns of *Fz6* Expression in Follicle-Associated Structures. Any model for the flow of polarity information in the skin must account for the temporal order in which different dermal structures develop. That is, if structure A develops and assumes its correct orientation before the appearance of structure B, then we can envision polarity information flowing from A to B but not the reverse. Similarly, Fz6-dependent polarity information can flow from structures that express Fz6 to those that do not, but this type of information cannot flow in the reverse direction. To explore these constraints, we defined the time course of development and the pattern of Fz6 expression for hair follicles, sebaceous glands, APMs, Merkel cell clusters, and sensory nerves in back skin and sebaceous glands and hair follicles on foot skin (Fig. 7).

Our time course data confirm previous analyses for these structures (2, 10, 11, 13, 21, 28), which demonstrated that follicles, sensory afferents, and Merkel cell clusters develop prenatally, whereas APMs and sebaceous glands develop postnatally (Fig. 7). APM development begins at ∼P1 with the secretion of the basement membrane protein nephronectin by bulge cells, the site of attachment of the APM on the follicle, and with the adjacent condensation of α8/β1 integrin-expressing dermal mesenchyme cells, the precursors of the APM (13). By ∼P6, fully differentiated APMs spanning from follicle to epidermis are seen by staining for SMA (Fig. 7 *A–C*). We note that differences between body regions and between different follicle types mean that a single time line of skin development represents an idealization and serves only to approximate the timing of events for any particular location.

Fz6 expression was analyzed by taking advantage of the nuclear localization signal (nls) *lacZ* reporter that was knocked into the *Fz6* locus. Anti–β-galactosidase immunostaining and/or X-gal histochemistry shows *Fz6* expression in epidermis, hair follicles, Merkel cells, and sebaceous glands, but not in APMs or DRG neurons, the source of sensory afferents (Fig. 7 *A–F*, *K*, and *M*). Close examination of X-gal–stained *Fz6*^{nlslacZ} DRGs shows that *Fz6* expression is confined to the vasculature (Fig. 7*K*). However, the closely related *Fz3* gene [analyzed in a similar fashion with a *lacZ* knock-in allele (29)] is expressed in DRG neurons starting before birth (Fig. 7*L*), raising the possibility that cutaneous sensory afferents might use Fz3-based rather than a Fz6-based polarity information to regulate the orientations of follicle associated sensory endings. *Fz3* is not detectably expressed in epidermis, hair follicles, or any other cells in the skin (Fig. 7*N*).

Taken together, the data suggest that early-developing and *Fz6*-expressing hair follicles and Merkel cells likely have direct access to *Fz6*-dependent polarity information, and late-developing and *Fz6*-nonexpressing APMs may receive polarity information secondarily from hair follicles and/or the epidermis. As sebaceous glands are also late to develop and form as an outgrowth from the follicle, their orientation is very likely derivative to that of the parent follicle. Whether cutaneous sensory endings have access to polarity information independent of the follicle with which they associate is uncertain, but the close match between the orientation of individual follicles and their associated C-shaped endings argues that nerve endings can distinguish the apical and basal faces of hair follicles and can use this distinction to direct their association with the target follicles.

Discussion

Coordination of Polarity Among Multicellular Structures. The experiments presented here reveal a previously unappreciated plasticity in the orientations of multicellular structures that, together with the follicle itself, comprise the hair follicle unit: sebaceous glands, APMs, Merkel cells, and afferent nerve terminals. The heterogeneity in follicle orientations seen in *Fz6*$^{-/-}$ mice facilitates the analysis of this phenomenon, because the combination of variable starting orientations and large reorienting movements permit a clear assessment of the extent to which the follicles and their associated structures coordinate orientations. We presume that the same plasticity exists in WT mice, the only difference being that, in WT hair follicle units, reorientation is generally limited to relatively small angular adjustments.

The different developmental schedules of follicle-associated structures and their different responses to the misorientation and reorientation of hair follicles suggest that polarity information is communicated among these structures in distinct ways. The simplest pattern is seen with sebaceous glands, which form after most follicle movement has already occurred and which arise as a direct outgrowth from the follicle. It is therefore not surprising

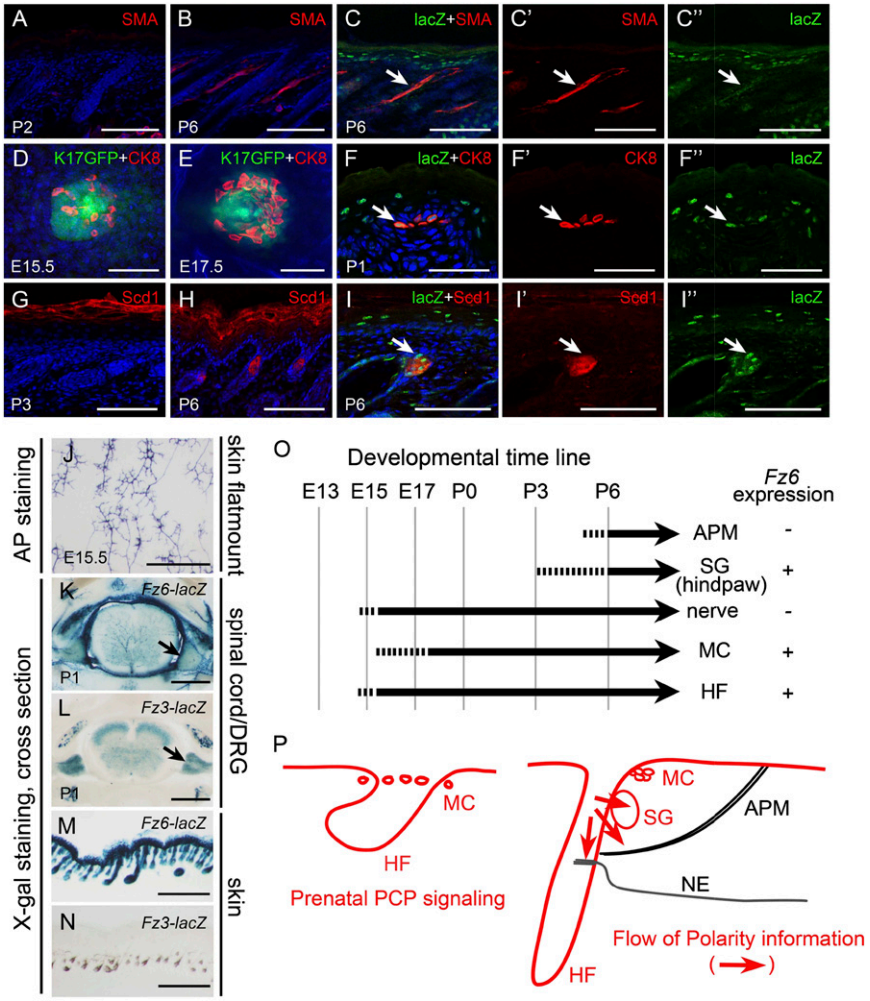

Fig. 7. Time course of development of follicle-associated structures and the expression pattern of *Fz6*. (*A–I*) Time of appearance of follicle associated structures: APMs (*A* and *B*), Merkel cells (*D* and *E*), and sebaceous glands (*G* and *H*), as revealed by SMA, cytokeratin 8, and Scd1 (34) immunostaining, respectively. Double immunostaining shows *Fz6* expression in Merkel cells (*F–F″*), sebocytes (*I–I″*) but not in APMs (*C–C″*). (*A–C* and *F–I*) Transverse skin sections with epidermis at top. (*D* and *E*) Skin flat mounts. (*J*) Morphology of sensory nerve endings in flatmounted back skin of E15.5 WT embryos visualized by sparse Cre-mediated recombination and AP staining of *Brn3a*$^{CKOAP/+}$;*NFLCreER* skin shows the initial stages of hair follicle innervation. (*K–N*) Patterns of *Fz3* and *Fz6* expression as determined by X-gal staining of P1 *Fz6*$^{nlacZ/+}$ and *Fz3*$^{lacZ/+}$ mice. Transverse vibratome sections through the spinal cord and DRGs show that in DRGs *Fz6* is only expressed in the vasculature and not in neurons (*K*), whereas *Fz3* is expressed in DRG neurons (*L*). Cross sections of skin showing that *Fz6* is expressed in skin and hair follicles but *Fz3* is not (*M* and *N*). X-gal staining of *Fz3*$^{lacZ/+}$ skin shows only melanin pigment. (*O*) (*Left*) Timeline summarizing the development of APMs, sebaceous glands (SG), sensory afferents, Merkel cells (MC), and hair follicles (HF). (*Right*) Summary of *Fz6* expression in the same structures. (*P*) Proposed flow of Fz6-dependent polarity information among follicle-associated structures. Hair follicle and Merkel cell (MC) polarity develops during prenatal life with direct input from the PCP system. The data suggest that sebaceous glands (SG), APMs, and nerve endings (NEs) receive polarity information (red arrows) from their associated hair follicles. (Scale bars, 100 μm in *A–C* and *G–I*; 50 μm in *D–F*; 500 μm in *J–N*.)

that sebaceous gland and follicle orientations are closely matched. The pattern of APM reorientation hints at a more complex program in which the site of APM attachment at the epidermis is either influenced by the orientation of a follicle tens to hundreds of micrometers away or can shift over time to accommodate follicle reorientation. A third pattern is shown by Merkel cells, which develop early, with groups of cytokeratin-8 positive epithelial cells coalescing around developing follicles by E17. In *Fz6*$^{-/-}$ mutants, the intrinsic polarity of Merkel cell clusters is absent. The expression of *Fz6* in developing Merkel cells, together with the demonstration that Merkel cells are of epithelial origin (12), suggests that the polarization of Merkel cell clusters may be determined by PCP signaling in the embryonic epidermis before the Merkel cells migrate below the keratinocyte monolayer. A fourth pattern is seen in the arrangement of melanocyte-rich zones in the tail skin. In *Fz6*$^{-/-}$ mutants, these zones exhibit disruptions in continuity and in location relative to hair follicle triplets on a spatial scale of several hundred micrometers. At present, little can be said about these structures, because it is not known whether *Fz6* is expressed in melanocytes or how the patterning of these melanocyte zones develops. Finally, the C-shaped follicle-associated sensory afferents show a response that appears to be a hybrid between the responses exhibited by APMs and Merkel cells, with some sensory afferents reorienting to accommodate the orientation of their target follicle and others switching from an asymmetric C-shape to a symmetric O-shape. Although correlative analyses of the type described here cannot define causal relationships, the data are consistent with the idea that hair follicles communicate their orientations to APMs and sensory afferents, which respond by reorienting appropriately.

Coordinating the spatial arrangement of multicellular structures is a ubiquitous feature of animal development. Among vertebrates, classic examples of ordered anatomic structures include the rostrocaudal arrangement of rib, vein, artery, and nerve within each segment of the thoracic wall; the arrangement of ligament and tendon insertion points on bones; and the microarchitecture of the inner ear. A fundamental question in such systems relates to the flow of information. In each case, one or more structures could direct the spatial arrangement of other interacting structures. Alternatively, the different structures could follow autonomous programs or pool information in a way that precludes a strictly hierarchical model. Ultimately, a full understanding requires a detailed description of the relevant molecular signals and cellular responses. At present, this level of understanding has not been fully realized for even the simplest model systems of cell–cell communication, such as the mother cell/forespore system of sporulating *Bacillus subtilis* (30).

Vertebrate Skin as a System for Studying Macroscopic Patterns. The present study showcases several experimental strengths of vertebrate skin and hair as a system for the quantitative analysis of tissue patterning. First, mutations that exclusively affect hair development or patterning, such as the *Fz6*-null mutation studied here, are not lethal, thereby facilitating a comparison of mutant and WT animals at all developmental stages. Second, the

number of hair follicles is large, and the structure of hair follicle units is stereotyped, features that permit the analysis of large data sets and facilitate the recognition of subtle affects on patterning. Third, skin is a relatively thin tissue that can by dissected intact and imaged as a flat mount with tissue-penetrating microscopy and/or clearing agents, thus preserving the spatial arrangements of large multicellular structures on the scale of the entire animal. Fourth, a large number of tissue stains, antibodies, and genetically directed cell marking methods have been developed for selectively visualizing a wide variety of skin structures. For completeness, we also note two additional experimental strengths arising from the surface location of skin that were not used in the present study: skin can be directly imaged in living animals and skin is highly amenable to experimental manipulation such as infection by transducing viruses to alter gene expression (31, 32). Taken together, these attributes make mammalian skin a uniquely attractive tissue in which to study the interaction of macroscopic and microscopic patterning systems.

Experimental Procedures

Mouse Husbandry. *Fz6*$^{+/-}$ and *Fz6*$^{-/-}$ mice were maintained on the background of a homozygous *K17-GFP* transgene. For *Fz6* genotyping, three primers were used: a shared forward primer (5′-CAAGCCATGTGGTAAAATCG-3′), a reverse primer in the endogenous *Fz6* coding region that is deleted in the targeted allele (5′-AGGCATGAAAATCCACTCAC-3′), and a reverse primer in the *nlacZ* coding region that is present in the *Fz6 KO* allele (5′-AAATTCAGACGGCAAACGAC-3′). The WT PCR product is 229 bp and the *Fz6 KO* product is 545 bp. *Fz6*$^{-/-}$*;ridge/ridge* mice could be typed by visual inspection of the hair pattern. *K17-GFP* transgenic mice were a kind gift of Pierre Coulombe (The Johns Hopkins University, Baltimore) (20); *Brn3a*^{CKOAP} mice are described in Badea et al. (33). This study was performed according to the approved Institutional Animal Care and Use Committee (IACUC) protocol M011M29 of the Johns Hopkins Medical Institutions.

Oil Red O staining. Hind paws from 3-wk-old mice were treated with commercial hair remover for 10 min and washed with tap water. Skins were dissected, pinned flat to Sylgard plates, fixed in 1% paraformaldehyde (PFA) in PBS for 30 min, rinsed in PBS, and then transferred to six-well plates for staining. Next, skins were washed in 60% isopropanol for 5 min, stained with 0.3% Oil red O in isopropanol for 2 h, rinsed with 60% (vol/vol) isopropanol for 5 min, and then stored in water before imaging. All of the procedures were performed at room temperature.

Immunostaining. For flat-mount immunostaining of P21 back skins, mice were treated with hair remover, wiped clean with tissue paper, and washed with tap water. Back skins were then dissected, rinsed with PBS, pinned flat to Sylgard plates, and fixed in 4% (wt/vol) PFA in PBS overnight at 4 °C. Skins were rinsed in PBS, washed with PBS containing 0.3% Triton X-100 (0.3% PBST) every 30 min for 5–8 h, and incubated with primary antibodies in 0.3% PBST containing 5% (vol/vol) goat serum and 20% (vol/vol) DMSO at room temperature for 5 d. Skins were then washed with 0.3% PBST every 30 min for 5–8 h and transferred to secondary antibodies in 0.3% PBST containing 5% goat serum and 20% DMSO and incubated at room temperature for 3 d. Skins were washed with 0.3% PBST every 30 min for 5–8 h, dehydrated in 25%, 50%, and 75% (vol/vol) methanol for 5 min and 100% methanol for 20 min three times, and then cleared in BBBA (benzyl benzoate, B-6630; Sigma and benzyl alcohol, 402834; 2:1; Sigma) overnight at room temperature. For flat-mount immunostaining of P1 back skin, skins were dissected, rinsed with PBS, pinned flat to Sylgard plates, and fixed in 2% (wt/vol) PFA in PBS at 4 °C for 2 h. Next, skins were rinsed in PBS, washed with 0.3% PBST for 30 min, and incubated with primary antibodies in 0.3% PBST containing 5% (vol/vol) goat serum overnight at 4 °C. Skins were then washed in 0.3% PBST for 30 min three times, incubated in secondary antibodies in 0.3% PBST at room temperature for 2 h, washed in 0.3% PBST, and flat mounted in Fluoromount G (17984-25; EM Sciences). For immunostaining on sections, skins were fixed in 2% (wt/vol) PFA for 2 h at room temperature, equilibrated with 30% (wt/vol) sucrose in PBS, and embedded in optimal cutting temperature compound (OCT). Frozen sections were cut at 10 μm and stained using the same protocol as for flat-mount immunostaining on P1 back skins except that the sections were incubated in secondary antibodies for 1 h. Primary antibodies were as follows: CK8 (TROMA-I-c; DSHB), 1:500; Neurofilament M (AB1987; Millipore), 1:1,000; GFP (A11122; Invitrogen), 1:2,000; α-SMA (C6198 Cy3 conjugated; Sigma), 1:400; β-galactosidase (rabbit, 5-prime/3-prime), 1:1,000; Scd-1 antibody (sc-14719), 1:150. Secondary antibodies were purchased from Invitrogen. Images were captured using a Zeiss SFM700 confocal microscope.

AM Dye Labeling. Acetoxymethyl ester (AM)1-43 (70024; Biotium) and AM4-65 (70039; Biotium) were dissolved in PBS and stored as 500 μg/mL stocks at −20 °C. For Merkel cell labeling, 10 μg of AM dye was injected into newborn pups s.c.. Back skins were collected 1 d later.

Tamoxifen Treatment and AP Histochemistry. To obtain sparse labeling of sensory nerves in the back skin, 1 mg tamoxifen (T5648; Sigma) was injected into pregnant females at E14.5. Back skins were collected at P2 or P21 for flat-mount AP histochemistry. Back skins were processed and stained with nitroblue tetrazolium/5-bromo-4-chloro-indolyl phosphate as described (26).

Angle Measurements and Statistical Analyses. Orientations of the symmetry axis of sebaceous gland pairs, APM bundles, nerve ending semicircles, and hair follicles was estimated by freely rotating a vector over the image and assessing the best fit by visual inspection. Angles were measured in Photoshop, and statistical comparisons were performed in Excel.

ACKNOWLEDGMENTS. We thank Hugh Cahill, Pierre Coulombe, Michael Deans, Xinzhong Dong, and Yanshu Wang for advice, materials, and/or helpful comments on the manuscript. This work was supported by The Howard Hughes Medical Institute.

1. Ross MN, Pawlina W (2011) Integumentary system. *Histology: A Text and Atlas* (Lippincott, Williams, and Wilkins, Philadelphia), pp 488–524.
2. Horsley V, et al. (2006) Blimp1 defines a progenitor population that governs cellular input to the sebaceous gland. *Cell* 126(3):597–609.
3. Nurse CA, Diamond J (1984) A fluorescent microscopic study of the development of rat touch domes and their Merkel cells. *Neuroscience* 11(2):509–520.
4. Boulais N, Misery L (2007) Merkel cells. *J Am Acad Dermatol* 57(1):147–165.
5. Woo SH, Stumpfova M, Jensen UB, Lumpkin EA, Owens DM (2010) Identification of epidermal progenitors for the Merkel cell lineage. *Development* 137(23): 3965–3971.
6. Maricich SM, et al. (2009) Merkel cells are essential for light-touch responses. *Science* 324(5934):1580–1582.
7. Ebara S, Kumamoto K, Matsuura T, Mazurkiewicz JE, Rice FL (2002) Similarities and differences in the innervation of mystacial vibrissal follicle-sinus complexes in the rat and cat: A confocal microscopic study. *J Comp Neurol* 449(2):103–119.
8. Li L, et al. (2011) The functional organization of cutaneous low-threshold mechanosensory neurons. *Cell* 147(7):1615–1627.
9. Fundin BT, et al. (1997) Comprehensive immunofluorescence and lectin binding analysis of intervibrissal fur innervation in the mystacial pad of the rat. *J Comp Neurol* 385(2):185–206.
10. Vielkind U, Sebzda MK, Gibson IR, Hardy MH (1995) Dynamics of Merkel cell patterns in developing hair follicles in the dorsal skin of mice, demonstrated by a monoclonal antibody to mouse keratin 8. *Acta Anat (Basel)* 152(2):93–109.
11. Peters EM, et al. (2002) Developmental timing of hair follicle and dorsal skin innervation in mice. *J Comp Neurol* 448(1):28–52.
12. Morrison KM, Miesegaes GR, Lumpkin EA, Maricich SM (2009) Mammalian Merkel cells are descended from the epidermal lineage. *Dev Biol* 336(1):76–83.
13. Fujiwara H, et al. (2011) The basement membrane of hair follicle stem cells is a muscle cell niche. *Cell* 144(4):577–589.
14. Goodrich LV, Strutt D (2011) Principles of planar polarity in animal development. *Development* 138(10):1877–1892.
15. Guo N, Hawkins C, Nathans J (2004) Frizzled6 controls hair patterning in mice. *Proc Natl Acad Sci USA* 101(25):9277–9281.
16. Devenport D, Fuchs E (2008) Planar polarization in embryonic epidermis orchestrates global asymmetric morphogenesis of hair follicles. *Nat Cell Biol* 10(11):1257–1268.
17. Ravni A, Qu Y, Goffinet AM, Tissir F (2009) Planar cell polarity cadherin Celsr1 regulates skin hair patterning in the mouse. *J Invest Dermatol* 129(10):2507–2509.
18. Wang Y, Badea T, Nathans J (2006) Order from disorder: Self-organization in mammalian hair patterning. *Proc Natl Acad Sci USA* 103(52):19800–19805.
19. Wang Y, Chang H, Nathans J (2010) When whorls collide: The development of hair patterns in frizzled 6 mutant mice. *Development* 137(23):4091–4099.
20. Bianchi N, Depianto D, McGowan K, Gu C, Coulombe PA (2005) Exploiting the keratin 17 gene promoter to visualize live cells in epithelial appendages of mice. *Mol Cell Biol* 25(16):7249–7259.
21. Müller-Röver S, et al. (2001) A comprehensive guide for the accurate classification of murine hair follicles in distinct hair cycle stages. *J Invest Dermatol* 117(1):3–15.
22. Alonso L, Fuchs E (2006) The hair cycle. *J Cell Sci* 119(Pt 3):391–393.
23. Plikus MV, Widelitz RB, Maxson R, Chuong CM (2009) Analyses of regenerative wave patterns in adult hair follicle populations reveal macro-environmental regulation of stem cell activity. *Int J Dev Biol* 53(5-6):857–868.

24. Linnet K (1993) Evaluation of regression procedures for methods comparison studies. *Clin Chem* 39(3):424–432.
25. Meyers JR, et al. (2003) Lighting up the senses: FM1-43 loading of sensory cells through nonselective ion channels. *J Neurosci* 23(10):4054–4065.
26. Badea TC, et al. (2012) Combinatorial expression of Brn3 transcription factors in somatosensory neurons: Genetic and morphologic analysis. *J Neurosci* 32(3):995–1007.
27. Rotolo T, Smallwood PM, Williams J, Nathans J (2008) Genetically-directed, cell type-specific sparse labeling for the analysis of neuronal morphology. *PLoS ONE* 3(12): e4099.
28. Van Keymeulen A, et al. (2009) Epidermal progenitors give rise to Merkel cells during embryonic development and adult homeostasis. *J Cell Biol* 187(1):91–100.
29. Wang Y, Thekdi N, Smallwood PM, Macke JP, Nathans J (2002) Frizzled-3 is required for the development of major fiber tracts in the rostral CNS. *J Neurosci* 22(19):8563–8573.
30. Higgins D, Dworkin J (2012) Recent progress in Bacillus subtilis sporulation. *FEMS Microbiol Rev* 36(1):131–148.
31. Beronja S, Livshits G, Williams S, Fuchs E (2010) Rapid functional dissection of genetic networks via tissue-specific transduction and RNAi in mouse embryos. *Nat Med* 16(7): 821–827.
32. Rompolas P, et al. (2012) Live imaging of stem cell and progeny behaviour in physiological hair-follicle regeneration. *Nature* 487(7408):496–499.
33. Badea TC, Cahill H, Ecker J, Hattar S, Nathans J (2009) Distinct roles of transcription factors brn3a and brn3b in controlling the development, morphology, and function of retinal ganglion cells. *Neuron* 61(6):852–864.
34. Harrison WJ, Bull JJ, Seltmann H, Zouboulis CC, Philpott MP (2007) Expression of lipogenic factors galectin-12, resistin, SREBP-1, and SCD in human sebaceous glands and cultured sebocytes. *J Invest Dermatol* 127(6):1309–1317.